

## The IRON Project: Photoionization of Fe ions

Sultana N Nahar

*The Ohio State University, Columbus, OH 43210, USA; nahar.1@osu.edu*

**Abstract.** The IRON Project, initiated in 1991, aims at two main objectives, i) study the characteristics of and calculate large-scale high accuracy data for atomic radiative and collisional processes, and ii) application in solving astrophysical problems. It focuses on the complex iron and iron-peak elements commonly observed in the spectra of astrophysical plasmas. The present report will illustrate the characteristics of the dominant atomic process of photoionization that have been established under the project and the preceding the Opacity Project and their importance in applications.

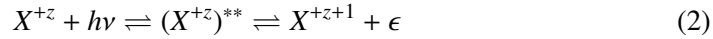
### 1. Introduction: Photoionization and the Opacity and Iron Projects

Photoionization, photo-excitation, electron ion recombination, electron impact excitation and ionization are the most dominant atomic processes in astrophysical plasmas. Modeling of astrophysical spectra for abundances, ionization fractions, diagnostics for the physical and chemical conditions, plasma opacity require the cross sections for photoionization when the plasma is around or near a radiative source, such as, a star.

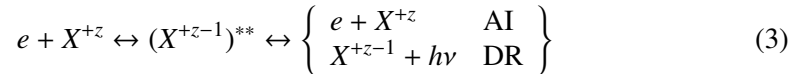
Photoionization process of an ion of charge  $+z$  can be direct:



This gives smooth background cross section. The process can be in two steps when an intermediate doubly excited state is formed:



In collisional description, an electron colliding with the ion can form an intermediate state where two electrons are excited. It is called an autoionizing state if it lies above the ionization threshold and breaks down either to autoionization (AI) when the electron goes free in a radiation-less process as the inner electron drops to the ground state or to dielectronic recombination (DR) when electron is captured by emission of a photon,



DR is the inverse of photoionization. The autoionizing state is a quantum state of energy

$$E_{xnl} = E(X^{+z}\nu l)^{**} = E_x - \frac{z^2}{\nu^2} = E_x - \frac{z^2}{(n-\mu)^2} \quad (4)$$

where  $E_x$  is an excited state of the residual or core ion relative to its ground state,  $nl$  is the quantum level of the outer electron.  $n$  is basically the effective quantum number  $\nu = n - \mu$  where  $\mu$  is the quantum defect describing the departure from a hydrogenic state. An autoionizing state introduces a resonance in photoionization cross section ( $\sigma_{PI}$ ). Levels  $E_x nl$  with different  $nl$  below an excited threshold  $E_x$  form the Rydberg series. So to each excited state of the residual ion, there can be a series of Rydberg resonances which show similar structure. A resonance is different from the typical rise in the background cross section at an excited threshold energy of an inner shell of the core ion. Identification of resonances can be complex for overlapping Rydberg states belonging to different  $E_x$  lying close together where the interference can modify the structures. Also depending on the values of the excitation rate coefficients and interference the strength of the resonances may reduce. In addition Seaton resonances (Yan and Seaton 1987), different from a Rydberg resonance can form (discussed later).

The autoionization rate ( $A_a$ ) is high, about  $10^{15-16} s^{-1}$ , and remains the same for all effective quantum number of the Rydberg series of resonances. The radiative decay rate ( $A_r$ ), about  $10^{8-12} s^{-1}$  for low lying levels, but increases as  $\nu^3$  and becomes comparable to  $A_a$  near and below the excited threshold of the residual ion. Both rates can be comparable at lower  $\nu$  for highly charged He- and Li-like ions.

The Opacity Project (OP) (Seaton 1987, Opacity Project 1995, 1996) carried out the first systematic study of photoionization of the ground and many excited states of astrophysically important atoms and ions from H to Fe. The atomic and opacity data computed are available in databases TOPbase (TOPbase) and OPserver (OPserver) respectively. OP solved many longstanding astrophysical problems. However, recent advances in technology for experimental measurements and astrophysical observations require data of higher accuracy. Follow-up of the OP the IRON Project (IP) (Hummer et al 1993) includes relativistic fine structure effect to achieve it in the study of the collisional and radiative processes of the much needed elements, and for the iron and iron peak elements. A significant amount of calculated data obtained under the IP are available online at TIPbase (TIPbase) and at atomic data page NORAD-Atomic-Data (NORAD) at the Ohio State University.

This report presents a review of the features in photoionization established under the OP and the IP using iron ions as examples. These ions are being studied particularly to obtain accurate opacity in the sun. Opacity depends mainly on photoionization and photoexcitation and gives a measure of radiation absorption in the plasma. It is related to the elemental abundances which has been a longstanding problem for the sun (e.g. Asplund et al 2004, 2009, Bailey et al 2015, Nahar and Pradhan 2016).

## 2. Theory

The theoretical method used for the study of photoionization is the R-matrix method with close coupling (CC) approximation for the wavefunction expansion. (e.g. Berrington et al 1987, *Atomic Astrophysics and Spectroscopy* (AAS)). CC approximation is the most precise way to generate the resonances naturally. A complete treatment of photoionization can be found in the textbook AAS. A brief outline of the theory is given below for the general guidance of the readers. Under the OP and the IP the R-matrix method (e.g. Burke and Robb 1975, AAS) was extended extensively for calculating excited states, oscillator strengths, photoionization cross sections  $\sigma_{PI}$  (Seaton 1987, Hummer et al 1993, Berrington et al 1987, 1995). The R-matrix package of codes

under the IP include the relativistic fine structure effects in Breit-Pauli approximation giving the name of the method as Breit-Pauli R-matrix or BPRM method.

In the CC approximation the atomic system is represented by the 'target' or the 'core' ion with  $(N+1)^{th}$  electron as the interacting electron. The  $(N+1)^{th}$  electron may be bound ( $E < 0$ ) or in the continuum ( $E \geq 0$ ). The total wave function,  $\Psi_E$ , in a  $J\pi$  symmetry is expressed as

$$\Psi_{E(e+ion)} = A \sum_i \chi_i(\text{ion})\theta_i + \sum_j c_j \Phi_j, \quad (5)$$

where  $\chi_i$  is wavefunction of the core ion at specific level  $S_i L_i (J_i) \pi_i$  coupled with the  $(N+1)^{th}$  electron function  $\theta_i$ . The first sum is over the ground and excited states of the the core ion.  $A$  is the anti-symmetrization operator. The  $(N+1)^{th}$  electron with kinetic energy  $k_i^2$  corresponds to a channel labeled  $S_i L_i (J_i) \pi_i k_i^2 \ell_i (S L (J) \pi)$ . The  $\Phi_j$ s are bound channel functions of the  $(N+1)$ -electrons system that account for short range correlation not considered in the first term and the orthogonality between the continuum and the bound electron orbitals of the core ion. It is assumed that the core ion orbitals remain the same before and after ionization that is the system is described by a wavefunction in spherical coordinates centered on the heavy point like and spinless nucleus with electric charge number  $+z$ . The wavefunctions of the core ion can be obtained from configuration interaction atomic structure calculations, such as using the program SUPERSTRUCTURE (Eissner et al 1974, Nahar et al. 2003).

The relativistic Hamiltonian in the BPRM method is given by (e.g. AAS)

$$H_{N+1}^{BP} = \sum_{i=1}^{N+1} \left\{ -\nabla_i^2 - \frac{2Z}{r_i} + \sum_{j>i}^{N+1} \frac{2}{r_{ij}} \right\} + H_{N+1}^{mass} + H_{N+1}^{Dar} + H_{N+1}^{so}. \quad (6)$$

where the relativistic mass correction, Darwin and spin-orbit interaction terms are

$$H_{N+1}^{mass} = -\frac{\alpha^2}{4} \sum_i p_i^4, \quad H_{N+1}^{Dar} = \frac{Z\alpha^2}{4} \sum_i \nabla^2 \left( \frac{1}{r_i} \right), \quad H_{N+1}^{so} = Z\alpha^2 \sum_i \frac{\mathbf{l}_i \cdot \mathbf{s}_i}{r_i^3}. \quad (7)$$

respectively. The Hamiltonian has additional two-body interactions terms (e.g. Nahar et al 2003). The BPRM method includes part of their contributions and neglect of the magnetic interaction (i.e. mutual spin-orbit, spin-other-orbit and spin-spin) of the colliding/outer electron with the valence electrons of the core ion.

Substitution of  $\Psi_{E(e+ion)}$  in the Schrodinger equation  $H_{N+1} \Psi_E = E \Psi_E$  introduces a set of coupled equations. They are solved using the R-matrix method where the space is divided into two regions, the inner region of a sphere of radius  $r_a$  with the ion at the center and the outer region. The wavefunction inside is represented by an expansion. known as the R-matrix basis.  $r_a$ , is chosen large enough for the electron-electron interaction potential is zero outside it. Beyond  $r_a$  the wavefunction is treated as Coulombic by the perturbation from the long-range electric multipole potentials arising from the target orbitals and elaborate angular algebra.

The transition matrix element for the dipole transition is given by  $\langle \Psi_B | \mathbf{D} | \Psi_F \rangle$ , where  $\mathbf{D} = \sum_i r_i$  is the dipole operator and the sum is over the number of electrons;  $\Psi_B$  and  $\Psi_F$  are the initial bound and final continuum wave functions. The transition matrix

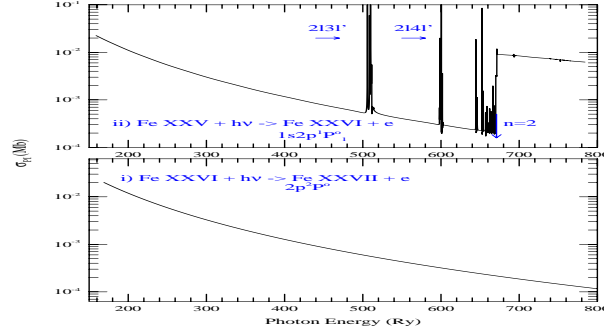


Figure 1. Photoionization cross sections  $\sigma_{PI}$  illustrating **i**) smooth decay of  $2p^2P^o$  state of H-like Fe XXVI and **ii**) resonant features in  $1s2p^1P^o$  state of He-like Fe XXV (Nahar et al 2001). The high peak resonances of type  $2l3l'$ ,  $2l4l'$  etc and enhancement in the background at the  $n=2$  threshold at 670 Ry have been introduced by the dipole allowed transition  $1s-2p$  in the core ion.

element can be reduced to generalized line strength as (e.g. AAS)

$$\mathbf{S} = |\langle \Psi_j | \mathbf{D} | \Psi_i \rangle|^2 = \left| \left\langle \psi_f \left| \sum_{j=1}^{N+1} r_j \right| \psi_i \right\rangle \right|^2, \quad (8)$$

where  $\Psi_i$  and  $\Psi_f$  are the initial and final state wave functions. The photoionization cross section ( $\sigma_{PI}$ ) is proportional to the generalized line strength as,  $\sigma_{PI} = \frac{4\pi^2}{3c} \frac{1}{g_i} \omega \mathbf{S}$ , where  $g_i$  is the statistical weight factor and  $\omega$  is the incident photon energy. The resonances are introduced by the interference in the transition matrix element of the bound wavefunction which includes core ion excitations and continuum wavefunction of the outer electron. For highly charged ions, radiation damping of autoionizing resonances can be treated using a scheme on fitting the dipole matrix of the autoionizing resonance (Sakimoto et al 1990, Pradhan and Zhang 1997, Zhang et al 1999)

### 3. Results and Discussions

Study of characteristic features of photoionization is important to learn the process and for precise applications. The central field or distorted wave approximations can be used to obtain the approximate background cross sections  $\sigma_{PI}$  (e.g. Reilman and Manson 1979, Gu 2008). The resonances computed separately were added to the background cross section (e.g. Simon et al 2010). The rate for the bound-free transition obtained from atomic structure rate can be broadened with a profile function to form the resonant shape. These can not demonstrate accurate features and can introduce large uncertainty. The following subsections illustrate features of  $\sigma_{PI}$  obtained from R-matrix method. Numerical notation is for an ion, such as Fe I for neutral and Fe II for  $\text{Fe}^+$ .

#### 3.1. Resonances in a two electrons system

A hydrogenic ion has no core electron and hence can not form a doubly excited autoionizing state for a resonance. The  $\sigma_{PI}$  of  $2p(^2P^o)$  state of H-like iron ion, Fe XXVI,

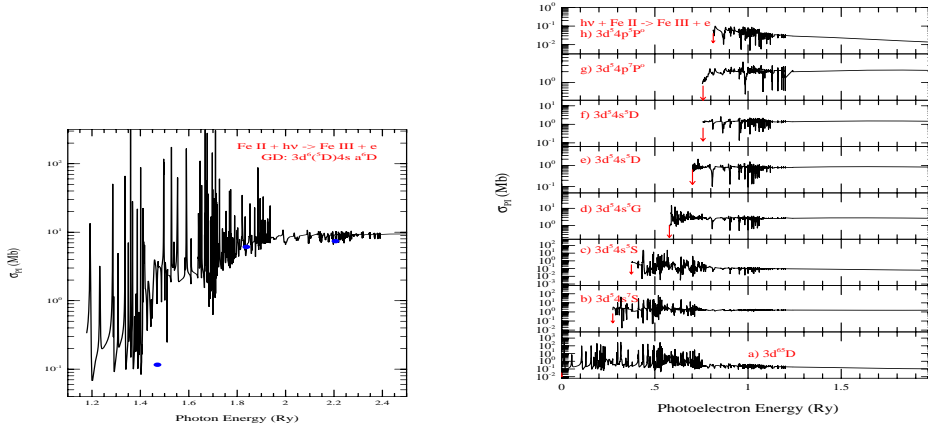


Figure 2. Left:  $\sigma_{PI}$  of the ground state,  $3d^6 4s^6 D$ , of Fe II demonstrating extensive resonances in the low energy region due to strong electron-electron interaction among 25 electrons (Nahar and Pradhan 1994). The blue points are from central field approximation (Reilman and Manson 1979). Right: Partial  $\sigma_{PI}$  of the ground state  $3d^6 4s^6 D$  for leaving the core ion in the ground (a) and 7 other excited states (b-h, thresholds pointed by arrows) as specified in the panels.

in Figure 1 (i) shows smooth decay with photon energy (Nahar et al 2001). The  $\sigma_{PI}$  for the  $1s2p(^1P^o)$  state of the He-like iron ion, Fe XXV (Figure 1 ii), decays like a hydrogenic ion at lower energy (shown beyond the ionization threshold energy 159 Ry to elaborate the resonances), but exhibits strong high peak resonances of type  $2l3l'$ ,  $2l4l'$  etc belonging to  $n=2$  states of the core ion (Nahar et al 2001). Considerable enhancement is seen at the excited  $n=2$  threshold energy of about 670 Ry (pointed by an arrow) due to dipole allowed  $1s - 2p$  transition in the core ion. These features have been generated by the BPRM method using a 10-CC wavefunction expansion or 10 levels of the core ion which can be excited up to 4f level. These structures were not found in the earlier work using a 1-state calculations under the OP (Seaton in TOPbase).

### 3.2. Resonances in ions with large number of electrons

Increasing number of electrons in the core ion usually increases number of excitations in the lower energy region and hence the number of Rydberg series of autoionizing resonances near the ionization threshold. These resonances are important for low to medium high temperature plasmas for integrated quantities containing an exponential factor such as recombination rates. Seaton resonances (shown later) are usually more prominent in the high energy and has more impact on high temperature plasmas.

Figure 2 (left panel) shows  $\sigma_{PI}$  of the ground state,  $3d^6 4s^6 D$ , of Fe II obtained from the largest atomic calculations at that time (Nahar and Pradhan 1994). The wavefunction expansion included 83 states from  $n=2,3$  complexes of the core ion Fe III. The ion shows strong electron-electron correlation interaction effect by generating extensive resonances near the ionization threshold and over the energy range of about 1.3 Ry inclusive of the 83 states. The earlier  $\sigma_{PI}$  obtained under the OP (Sawey and Berrington 1992) had incomplete correlation interaction and produced only the general background which is much lower than the present values.

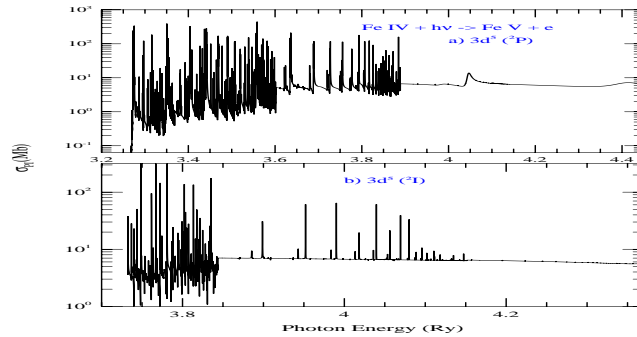


Figure 3.  $\sigma_{PI}$  of two equivalent states  $3d^5(^2P)$  and  $3d^5(^2D)$  of Fe IV (Nahar 2005) demonstrating continuing dominance of the background at higher energies.

The total  $\sigma_{PI}$ , such as that of Fe II above, is obtained by summing up the partial  $\sigma_{PI}$  corresponding to ionization leaving the residual ion at the ground and various excited states. With increase of photon energy the ion is ionized with higher excitations of the core ion. Right panel of Figure 2 presents partial  $\sigma_{PI}$  with resonant structures leaving the residual ion at the ground (a) and 7 (b-h) other lower excited states (Nahar and Pradhan 1994). The partial cross sections help in identification of the resonances.

### 3.3. Photoionization of excited equivalent electron states

The ground state photoionization typically has less features than those of excited states. (Fe II in Figure 2 is an exception) and slow decay of the background cross section. The other states that show slow decay of the background  $\sigma_{PI}$  are the equivalent electron states. However, they have more resonant features in the lower energy region. These states are important contributor to processes relevant to it, such, electron-ion recombination. Figure 3 presenting  $\sigma_{PI}$  of two equivalent electron states of Fe IV (Nahar 2005) obtained using a 16-CC wavefunction expansion (Nahar and Pradhan 2005) shows the typical features of equivalent electron states. Narrow Rydberg resonances belong to various low lying excited states of the core ion form prominently at and near the ionization threshold and the background continues to remain high beyond the highest excitation threshold of the core ion included in the wavefunction expansion. Equivalent electron states do not show the wide Seaton resonances (illustrated belows)

### 3.4. Seaton Resonances due to PEC

A Seaton resonance is different from a Rydberg resonance. It forms in  $\sigma_{PI}$  of an excited state "i" with a single valence electron. The core ion at ground state absorbs the photon for photo-excitation-of-core (PEC) to a dipole allowed state of transition of energy  $Ex$ . The outer electron remains inactive temporarily or a "spectator" during the transition but leads to ionization as the excited core ion drops to the ground state. PEC interferes with the Rydberg resonances and manifests as a wider resonance with enhanced background, often by orders of magnitude, at an energy of  $Ex - Ei$  from the ionization threshold energy  $Ei$  of the state "i". Figure 4 illustrates characteristics of a Seaton resonance (pointed by arrow) in  $\sigma_{PI}$  (Nahar 1996) - of the excited  $3d^5(^6S)7p(^5P^o)$  state (left) and of a number of excited states of Fe III (right). A Seaton resonance is more

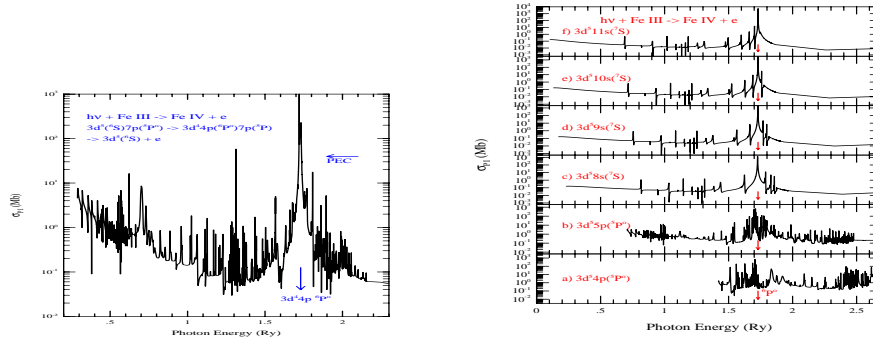


Figure 4. Left:  $\sigma_{PI}$  of the excited  $3d^5(6S)7p(5P^o)$  state of Fe III exhibiting huge Seaton resonance at 1.73 Ry, the transition energy for a PEC from the ground  $3d^5(6S)$  to excited  $3d^44p(6P^o)$  state of the core ion Fe IV. Right:  $\sigma_{PI}$  of two series of excited states of Fe III - a)  $3p^54p(5P^o)$ , b)  $3p^55p(5P^o)$ , and c)  $3p^58s(7S)$ , d)  $3p^59s(7S)$ , e)  $3p^510s(7S)$ , f)  $3p^511s(7S)$  illustrating that regardless of the state, the energy position (pointed by arrow) of a Seaton resonance remains the same (Nahar 1996).

distinct in higher excited states Figure 4 (right, b-f). Interference from electron-electron correlation of low lying excited states can reduce the prominence of the structure and may appear slightly shifted Figure 4 (right, a,b). Seaton resonances cause the high energy behavior of  $\sigma_{PI}$  non-hydrogenic for low to fairly high lying excited states contradicting their assumed hydrogenic  $1/\nu^3$  behavior with energy.

### 3.5. Resonances at and near ionization threshold due to relativistic channels

Relativistic effects are important when electrons are moving very fast due to high nuclear charge of a heavy or high  $Z$  element and highly charged ion, such as, Fe XXV. Relativistic effects break the resonances in to fine structure components causing narrower and larger number of resonances. However, we have found that fine structure effect can introduce strong resonances at and near ionization threshold region of  $\sigma_{PI}$  for low to medium high  $Z$  elements (e.g. for P II by Nahar et al 2017) but not significant for the rest of the energy region. Figure 5 presents  $\sigma_{PI}$  of  $2s2p^3(5S^o)$  of carbon like Fe XXI demonstrating the relativistic fine structure effect introducing strong resonances in the near threshold region not allowed in LS coupling approximation (Nahar 2008). In LS coupling the state  $2s2p^3(5S^o)$  photoionizes only to  $2s2p^2(4P)\epsilon d(5P)$  or  $2s2p^2(4P)\epsilon ns(5P)$  and leave the core ion at  $2s2p^2(4P)$  state. It means that  $\sigma_{PI}$  is zero below the  $4P$  state (pointed by an arrow in Figure 5). However, in reality resonances can form below the  $4P$  threshold by the fine structure couplings effect. The fine structure channels with the excited core ion,  $2s2p^2(4P)nd, ns(5P_{1,2,3})$ , are allowed to couple with those of the ground levels  $2s^22p^2(2P^o_{1/2,3/2})\epsilon p(1,3P_{1,2,3})$ . This leads to radiationless autoionization below the  $4P$  threshold and introduction of the narrow and high peak resonances almost zero background cross section (Nahar 2008). These resonances have found to make significant contribution to low temperature plasmas.

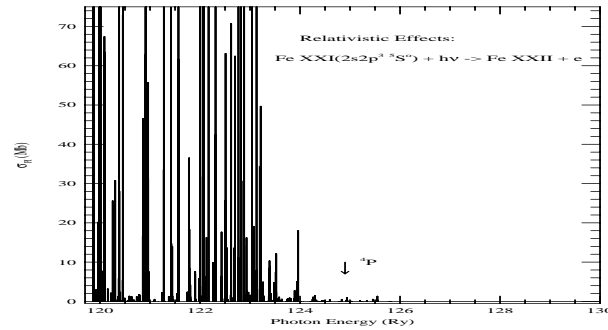


Figure 5.  $\sigma_{PI}$  of the excited  $2s2p^3(^5S^o)$  state of Fe XXI showing narrow, high peak resonances below the first excited core ion threshold  $2s2p^2(^4P)$  (pointed by arrow) formed by fine structure couplings (Nahar 2008).

### 3.6. Resonant enhancement due to $\Delta n=1$

The wavefunction expansions considered by the OP included core ion states from the  $n$ -complex of the outer electron, i.e.  $\Delta n = 0$ . It was assumed that the high lying states i) are not common in astrophysical plasmas of interest and ii) have weak couplings to lower ones causing weaker resonances. However, it included the rise in the decaying  $\sigma_{PI}$  at an inner shell ionization threshold of the core ion. The later studies (e.g. for oxygen ions Nahar 1998) found that resonances due to high lying the core ion states with  $\Delta n=1$  are much stronger with high peaks than those with  $\Delta n=0$  states. Hence without their consideration, integrated cross section can be underestimated.

Figure 6 presents  $\sigma_{PI}$  of the excited  $2s^22p3d(^3D^o)$  state of Fe XXI obtained using (a) a 29-CC wavefunction expansion that includes  $\Delta n = 0,1$  states (Nahar 2008a) and (b) a 8-CC expansion which includes  $\Delta n = 0$  states only (Lou and Pradhan 1989). The first complex of narrow Rydberg resonances (with arrow at  $n=2$ ) belong to excitations of the core ion to  $\Delta n=0$  states, that is to states with  $n=2$ . They are less prominent than those arising from  $n=3$  states in the higher energy region where the features are more extensive and stronger spanning over a larger energy range. The latter can be divided into two groups: the broader Seaton resonances in the photon energy range of 73 to 82 Ry by 8 possible PECs and series of narrow Rydberg resonances belonging to various states of  $n=3$  complex in the rest of the high energy region. The high energy background has also enhanced considerably. Such prominent effects were not unexpected for Fe XXI because of the large energy gap of about 50 Ry between  $n=2$  and 3 states. The prominence can be explained by the larger radiative decay rates for  $n=3$  states.

### 3.7. Convergence of enhancement due to Resonances

Photoionization of Fe XVII was studied to determine the impact of  $\Delta n = 2$  excitations in the core ion. The  $\sigma_{PI}$  of the ion contributes significantly to the opacity of the plasma near the boundary between radiative and convection zones of the sun.  $\sigma_{PI}$  with a wavefunction of 60 fine structure levels (30 LS states) with  $\Delta n=0,1$  showed considerable amount of photoabsorption (Nahar et al 2011) (e.g.  $\sigma_{PI}$  in black for the  $2s^2p^53d(^1D^o)$  state of Fe XVII in Figure 7) not seen with those using a 2-CC wavefunction (Scott, TOPbase, blue in the figure). The enhancements in  $\sigma_{PI}$  from 60-CC increased the



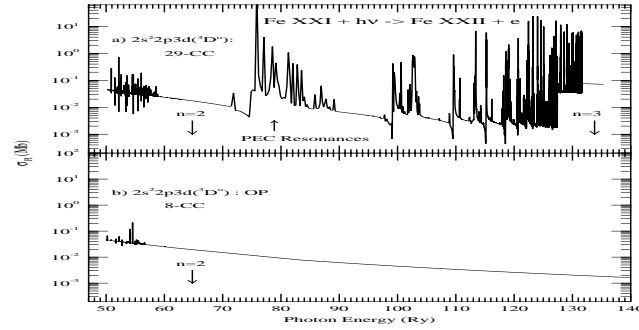


Figure 6. Effect of core ion excitations on  $\sigma_{PI}$  of the  $2s^2 2p 3d(^3D^o)$  state of Fe XXI to  $\Delta n = 0$  states (8-CC, Lou and Pradhan 1989) and to  $\Delta n = 1$  states (29-CC, Nahar 2008a) Comparison shows i) the wide Seaton resonances in the energy range of 73 - 82.5 Ry, ii) high peak resonances by stronger correlation effect, and iii) enhancement in the background at higher energy by the excitations to  $n=3$  states.

Rosseland mean opacity for Fe XVII by 20% from that of 2-CC and explained the possible reason for discrepancy with the measured values (Bailey et al 2015).

The latest study of  $\sigma_{PI}$  for Fe XVII (Nahar and Pradhan 2016) used a larger wavefunction expansion of 99 states covering the  $n=4$  states ( $\Delta n=0,1,2$ ) (red in Figure 7)). Arrows point the energy positions for the highest  $n=2, 3$ , and 4 states. We note no significant enhancement from  $n=4$  excitations, the resonances were much weaker and negligible enhancement in the background cross section (red) compared to those due to  $n=3$  states (black). These demonstrate that a convergence of resonant contributions from core excitations to higher  $n$  states has reached. The narrow resonances close to the ionization threshold in the black curve of 30-CC are from fine structure couplings of relativistic BPRM method. Such convergence with  $\Delta n = 2$  excitations in the core ion was also noted in  $\sigma_{PI}$  for Fe XXV (Nahar et al 2001).

### 3.8. Resonances below K-Shell ionization

Resonances below the last ionization threshold, the K-shell threshold, may show multiple ionization effect. Typically resonances become weaker and background will drop with higher photon energy. However, resonances below the K-shell, tend to rise again due to the higher  $1s-2p$  excitation rates. Their peaks can be orders of magnitude higher than the rise in K-shell ionization threshold and the background, such as, over 2 orders of magnitude for Fe and over 3.5 orders for AU as presented in Figure 8 (Pradhan et al. 2009, Lim et al. 2012). Figure 8 shows these resonances added to the background cross sections of the atoms available at the website of NIST (NIST2). The complex of resonances in Figure 8 correspond to allowed  $K_\alpha$  ( $1s-2p$ ) transitions of all ionization stages from Ne- to He-like ion following K-shell ionization. In the Auger process, where an L-shell electron drops down to fill the K-shell vacancy, a  $K_\alpha$  photon is emitted. This photon can knock out an L-shell electron creating an additional hole there. Continuation of such process to higher levels can lead to Coster-Kronig cascading, that is, multiple ionization stages as photons and electrons are ejected out. However, such cascade can occur if the photon energy matches to those of the resonances presented

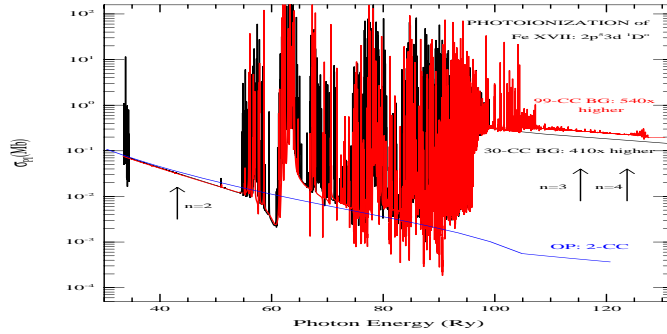


Figure 7. Comparison of  $\sigma_{PI}$  of the excited  $2s^2 2p^5 3d^1 D^o$  state of Fe XVII from the three calculations, i) 2-CC in blue (scott), ii) 30-CC (60 fine structure levels) in black (Nahar et al. 2011) and iii) 99-CC in red (Nahar and Pradhan 2016). The high peak strong resonances and huge background enhancement by orders of magnitude are due to  $\Delta n=1$  states in the wavefunction. The weaker resonances of  $n=4$  excitations indicate the convergence of resonant contributions with higher  $n$ . The arrows indicate the energy limits for the  $n=2,3,4$  states of the core ion.

in the figure (Pradhan et al 2009). The enhanced resonant photoionization can result in resonant  $K_\alpha$  fluorescence below the K-shell ionization of each ionization stages of Ne-like to He-like ions and was observed by Vinko et al. for Al (2012) and interpreted by Nahar and Pradhan (2015).

#### 4. Accuracy and Completeness

Both accuracy and completeness are needed for calculations of photoionization cross sections for precise prediction in features, benchmarking with high precision experiment, and applications for solving problems. Accuracy depends on the number of states included in the wavefunction expansion, configurations included for accurate representation of correlation effect and number of points for delineation of the resonances. Completeness means obtaining cross sections for large number of bound states. These have been objectives of both the OP and the IP. An example of accuracy is given in Figure 9 presenting  $\sigma_{PI}$  of the complex ion P II where the combined resonant features observed in the sophisticated set-up of Advanced Light Source in Berkeley National Lab (panel a) are being identified with theoretical calculations using close coupling approximation and R-matrix method in panels b-f (Nahar et al 2017). Comparison shows that the observed features are reproduced in theory and that belong to those of the ground and low lying metastable levels.

#### 5. Conclusion

The extensive study of atomic photoionization carried out under the Iron Project and the Opacity Project has established number of characteristic features of the process. They have critical impact on the astrophysical applications, such as, determination of the plasma opacity, elemental abundances, ionization fractions. Detailed study of the

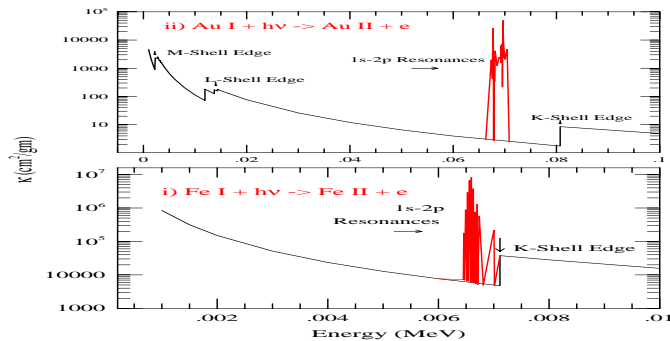


Figure 8. High peak resonances below the K-shell ionization threshold of i) iron and ii) gold arising from  $K_{\alpha}$  ( $1s-2p$ ) transitions. The resonances correspond to all allowed  $K_{\alpha}$  transitions of the Ne- to He-like ions as the element goes through multiple ionization stages at a resonant energy (Pradhan et al 2009).

process with high accuracy and compute large scale atomic data for completeness are necessary for precise analysis of astrophysical spectra and in other applications.

**Acknowledgments.** Partial support by DOE grant DE-FG52-09NA29580 and NSF grant AST-1312441. Computations were carried out at the Ohio Supercomputer Center

## References

- Asplund M, Grevesse N, Sauval J, arXiv 2004;astro-ph/0410214v2  
 Asplund M, Grevesse N, Sauval J, Scott P, *Annu. Rev. Astron. Astrophys.* 47, 481-522 (2009)  
 Bailey et al. (22 authors) *Letter, Nature* 517, 56 (2015)  
 Berrington KA, Burke PG, Butler K, et al, *J. Phys. B* 20, 6379 (1987)  
 Berrington KA, Eissner W, Norrington PH, *Comput. Phys. Commun.* 92, 290 (1995)  
 Burke PG, Robb WD, *Adv. At. Mol. Phys.* 11, 143-214 (1975)  
 Eissner W, Jones M, & Nussbaumer H, *Comput. Phys. Commun.* 8, 270-306 (1974)  
 Gu MF, *Can. J. Phys.* 86, 675-689 (2008)  
 Hummer, D.G., Berrington, K.A., Eissner, W., et al, *Astron. Astrophys.* 279, 298-309 (1993)  
 Lim S, Montenegro M, Pradhan AK, Nahar SN, Chowdhury E, Yu Y, *World Congress on Med. Phys. Biomed. Eng., IFMBE Proceedings* 39, p. 2248 (Ed. M. Long, Springer, 2012)  
 Luo D, Pradhan AK, *J Phys B* 22, 3377-95 (1989)  
 OPSERVER: Mendoza C, Seaton MJ, Buerger P, et al. *MNRAS* 378, 1031 (2007). Data at <http://opacities.osc.edu>.  
 Nahar SN, *Phys. Rev. A* 53, 1545-1552 (1996)  
 Nahar SN, *Phys. Rev. A* 58, 3766 (1998)  
 Nahar SN, *J. Quant. Spec. Rad. Transfer* 109, 2731-2742 (2008)  
 Nahar SN, *J. Quant. Spec. Rad. Transfer* 109, 2417-2426 (2008)  
 Nahar SN, unpublished, Results obtained using the wavefunction of Nahar SN, Pradhan AK, 437, 345 (2005)  
 Nahar SN, Eissner W, Chen GX, Pradhan AK. *A&A* 408, 789-801 (2003)  
 Nahar SN, Hernández EM, Hernández L, et al. *JQSRT* 187, 215-223 (2017)  
 Nahar SN, Montenegro M, Eissner W, Pradhan AK, *Phys. Rev. A* 82, Brief Rep 065401 (2010)  
 Nahar SN, Pradhan AK, Montenegro K, in *Simulations in Nanobiotechnology*, CRC Press - Taylor & Francis group, Chap 9, p.305-330 (2011)  
 Nahar SN, Pradhan AK, *J. Phys. B* 27, 429 (1994)

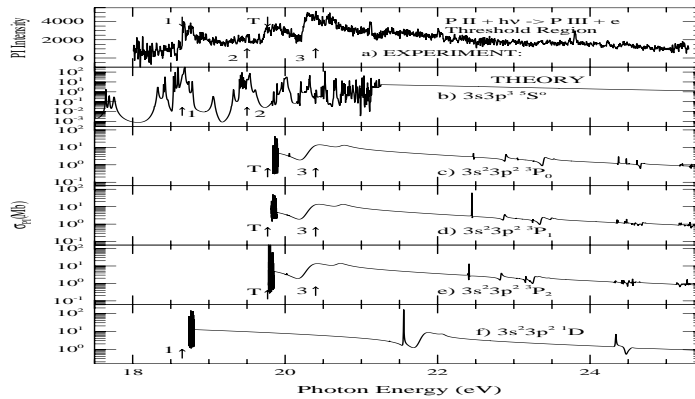


Figure 9. Benchmarking of  $\sigma_{PI}$  of P II for accuracy: (a) the combined features observed in experiment, (b-f) theoretical identification of observed features (1,2,3,T) generated by the (b) excited level  $3s3p^3(^5S_2^o)$ , (c) ground level  $3s^2 3p^2(^3P_0)$  and (d,e,f) the three excited levels  $3s^2 3p^2(^3P_{1,2})$ ,  $3s^2 3p^2(^1D_2)$ . Agreement is seen in reproducing the observed features (Nahar et al 2017)

- Nahar SN, Pradhan AK, *Astron. Astrophys* 437. 345 (2005)  
 Nahar SN, Pradhan AK, Chen GX, Eissner W, *Phys. Rev. A* 83, 053417 (2011)  
 Nahar SN, Pradhan AK, Zhang HL, *Astrophys. J. Suppl.* 133, 255 (2001)  
 Nahar SN, Pradhan AK, *QSR* 155, 32-48 (2015)  
 Nahar SN, Pradhan AK, *Phys. Rev. Lett.* 116, 235003 (2016)  
 NIST2: <http://physics.nist.gov/PhysRefData/Xcom/html/xcom1.html>  
 NORAD atomic data website: <http://norad.astronomy.ohio-state.edu>  
 Pradhan, A.K. & Nahar S.N. in *Atomic Astrophysics and Spectroscopy* (AAS) (Cambridge University press, 2011)  
 Pradhan AK, Nahar SN, Montenegro N, et al *J. Phys. Chem. A* 113, 12356 (2009)  
 Pradhan AK & Zhang HL, *J. Phys. B* 30, L571-L579 (1997)  
 R.F. Reilman and S.T. Manson, *Astrophys. J. Suppl.* **40**, 815 (1979)  
 Sakimoto K, Terao M, & Berrington K.A, *Phys. Rev. A* 42, 291-295 (1990)  
 Sawey PMJ, Berrington KA, *J. Phys* 8: *At. Mol. Opt. Phys* 25 (1992) 1451-1466  
 Scott MP; unpublished, data in TOPbase  
 Seaton, M.J., *J. Phys. B*, 6363-6378 (1987)  
 The Opacity Project Team. *The Opacity Project*, Vol 1, 1995, Vol. 2, 1996, Institute of Physics  
 Seaton MJ, unpublished, data available at TOPbase  
 Simon MC, Schwarz M, Epp SW, et al, *J. Phys. B: At. Mol. Opt. Phys.* 43 065003 (2010)  
 TIPbase: <http://cdsweb.u-strasbg.fr/tipbase/topbase.html>  
 TOPbase: <http://cdsweb.u-strasbg.fr/topbase/topbase.html>  
 Vinko SM, Ciricosta O, Cho BI, et al., *Nature* 482, 59 (2012)  
 Yu Y. & Seaton, M.J. *J. Phys. B* 20, 6409-6429 (1987)  
 Zhang HL, Nahar SN, Pradhan AK. *J. Phys. B* 32, 1459-1479 (1999)